

Non-hydrogenic excitons in perovskite $\text{CH}_3\text{NH}_3\text{PbI}_3$

E. Menéndez-Proupin,^{1,2} Carlos L. Beltrán Ríos,³ and P. Wahnón²

¹*Departamento de Física, Facultad de Ciencias, Universidad de Chile, Casilla 653, Santiago, Chile*

²*Instituto de Energía Solar and Dept. TFB, E.T.S.I. Telecomunicación, Universidad Politécnica de Madrid, Spain*

³*Escuela de Física, Universidad Industrial de Santander, A. A. 678, Bucaramanga, Colombia*

(Dated: July 3, 2015)

The excitons in the orthorhombic phase of the perovskite $\text{CH}_3\text{NH}_3\text{PbI}_3$ are studied using the effective mass approximation. The electron-hole interaction is screened by a distance-dependent dielectric function, as described by the Haken potential or the Pollmann-Büttner potential. The energy spectrum and the eigenfunctions are calculated for both cases. The effective masses, the low and high frequency dielectric constants, and the interband absorption matrix elements, are obtained from generalized density functional theory calculations. The results show that the Pollmann-Büttner model provides better agreement with the experimental results. The discrete part of the exciton spectrum is composed of a fundamental state with a binding energy of 24 meV, and higher states that are within 2 meV from the onset the unbound exciton continuum. Light absorption is dominated by the fundamental line with an oscillator strength of 0.013, followed by the exciton continuum. The calculations have been performed without fitting any parameter from experiments and are in close agreement with recent experimental results.

Keywords: metal halide perovskite, polaron, dielectric, Wannier-Mott exciton, Haken exciton, Pollmann-Büttner exciton

Hybrid organic/inorganic perovskites based on lead or tin tri-halides are semiconductor materials that have revolutionized the research of thin film solar cells. With the first prototypes demonstrated six years ago,¹ record cell efficiencies have surpassed the barrier of 20%.^{2,3} Methylammonium lead iodide ($\text{CH}_3\text{NH}_3\text{PbI}_3$) is one of the most studied members of this family, and it has been applied as photon absorber and charge transporting material.^{4,5}

$\text{CH}_3\text{NH}_3\text{PbI}_3$ presents two phase transitions at ~ 162 K and ~ 327 K. At these transitions, the crystal symmetry changes first from orthorhombic to tetragonal and then to cubic symmetry.⁶⁻⁹ The three phases differ by small changes of the lattice vectors, rotations of the characteristic PbI_6 octahedra, and the orientation of the CH_3NH_3^+ cations. In the tetragonal and cubic phases, the CH_3NH_3^+ cations present orientational and dynamic disorder,¹⁰ with a deep effect on the dielectric properties.^{11,12} In the low temperature orthorhombic phase, the CH_3NH_3^+ positions and orientations are fixed.^{6,7}

The electronic band structure of $\text{CH}_3\text{NH}_3\text{PbI}_3$ has been explained on the basis of generalized density functional theory (hybrid functionals) or Green functions GW calculations, in both cases including the spin-orbit coupling.¹³⁻¹⁵ For the orthorhombic phase, the valence band maximum (VBM) and the conduction band minimum (CBM) are located at the Γ point corresponding to the 48-atoms unit cell, and the fundamental gap is 1.68 eV.¹⁶ Both the VBM and CBM are doubly degenerated, with nearly symmetric effective mass tensors.

Exciton peaks are observed in the light absorption spectra at low temperature,¹⁷⁻¹⁹ just below the interband absorption edge, or melded with it, depending on the temperature. According to the Wannier-Mott model,^{20,21} the exciton is similar to a hydrogen atom with the proton and electron masses replaced by the hole and

electron effective masses, and the Coulomb interaction is screened by a dielectric constant ϵ . Therefore, the exciton binding energy and the Bohr radius are $Ry = \mu e^4 / 2\hbar^2 \epsilon^2$ and $a_{ex} = \hbar^2 \epsilon / \mu e^2$, where $\mu = m_e m_h / (m_e + m_h)$ is the reduced electron-hole mass.

One distinct feature of $\text{CH}_3\text{NH}_3\text{PbI}_3$ is the large difference between the static dielectric constant ϵ_0 and the high frequency constant ϵ_∞ , i.e., for frequencies higher than those of the phonon absorption. Values of ϵ_∞ in the range 4.5 – 6.5 have been calculated,^{13-15,22} while values close to 25 have been estimated for ϵ_0 .^{14,22} Such difference is larger than in traditional inorganic semiconductor and should cause important polaron effects, such as the effective mass and gap renormalization, as well as non-hydrogenic exciton states. For the latter, immediately arises the question whether the screening constant ϵ should be the static dielectric constant ϵ_0 or the high frequency ϵ_∞ . Using the values listed in Table I, the static and the high frequency dielectric constants lead to very different values of the exciton binding energy $Ry_0 = 2.8$ meV and $Ry_\infty = 50$ meV, respectively. Such different energies lead to different conclusions with respect to exciton dissociation due to thermal excitation, as well as to different interpretation of luminescence and transport properties.

Early estimations of the exciton binding energy^{17,18} $\sim 37-50$ meV were based on measurement of the exciton diamagnetic coefficient and interpretation based on the hydrogenic model with screening by $\epsilon_\infty = 6.5$. Recent studies of the temperature dependence of photoluminescence spectra,²³ and numerical analysis of the absorption spectra^{24,25} have provided updated exciton binding energies around 16-19 meV. The latter values point to a screening constant intermediate between ϵ_∞ and ϵ_0 . Even et al²⁴ fitted the absorption spectrum using the Wannier-Mott exciton model and obtained an effective

dielectric constant $\epsilon_{eff} = 11$.

In fact, the differences between ϵ_0 and ϵ_∞ express the electric polarization associated to the optical phonons and the electron-phonon interaction. The stationary states are coupled states of electronic and the vibrational phonon field. The quantum calculation of these coupled states is beyond the current capabilities of ab initio methods. Model Hamiltonians^{26–28} allow one to map the coupled electron-phonon excitations into effective electronic states, and to obtain the energies of stationary states. Even when simplifying approximations are inherent in the models, they can provide a criterium on the relevant dielectric screening constants. In this Article, we apply the model Hamiltonians of Haken^{26,27} and that of Pollmann and Büttner²⁸ to the exciton spectrum. This formalism is applicable to the low temperature orthorhombic phase because in the tetragonal phase the static dielectric increases strongly, associated to the re-orientation of CH_3NH_3^+ cations, and the exciton effects practically disappear.^{11,12,24,25}

The strength of the interaction of electrons and optical phonons is given by the coupling constant

$$\alpha_p = \sqrt{me^4/2\hbar^2\epsilon_*^2 E_{LO}}, \quad (1)$$

where E_{LO} is the energy of the longitudinal optical phonon. This model was developed for simple crystals that display one single LO phonon branch. For this application, we have chosen E_{LO} as the shift of the main peak in the $\text{CH}_3\text{NH}_3\text{PbI}_3$ Raman spectrum.²⁹ The ionic screening parameter appearing in Eq. (1) is $1/\epsilon_* = 1/\epsilon_\infty - 1/\epsilon_0$.

For transport properties, relevant after exciton dissociation, polaron masses must be considered rather than the bare electronic masses computed with fixed ions. They can be estimated using the Fröhlich's continuum theory of the large polaron,³⁰ which predicts

$$m^* = m \left(1 + \frac{\alpha_p}{6} \right).$$

The polaron bands undergo an additional shift given by $\Delta E_p = -\alpha_p E_{LO}$. With the data of Table I, this leads to a reduction of the electronic band gap by 95 meV.

The Haken model^{26,27} describes two interacting polarons, each one with a radius much smaller than the exciton effective radius, and expresses the effective potential for the electron-hole Coulomb interaction as

$$V_H(r) = -\frac{e^2}{\epsilon_0 r} - \frac{e^2}{2\epsilon_* r} \left(e^{-r/l_e} + e^{-r/l_h} \right). \quad (2)$$

Here $l_{e,h} = \sqrt{\hbar^2/2m_{e,h}E_{LO}}$ are the electron- and hole-polaron radii determined using bare band electron and hole effective masses. The polaron effective mass parameters must be used in the kinetic energy terms of the Hamiltonian.³¹

The model proposed by Pollmann and Büttner²⁸ (PB) takes into account the correlation between electron and

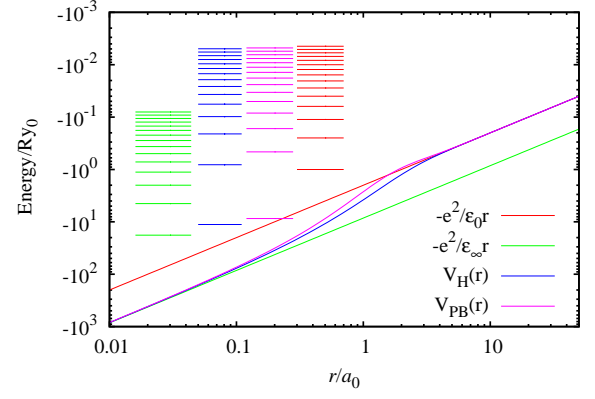


FIG. 1. Haken and PB potentials compared with the Coulomb potential screened by ϵ_0 and ϵ_∞ . Also shown are the eigen-energies for each potential.

hole polarons, and leads to corrections to the Haken potential. The resulting electron-hole interaction potential is

$$V_{PB}(r) = -\frac{e^2}{\epsilon_0 r} - \frac{e^2}{\epsilon_* r} \left(\frac{m_h}{\Delta m} e^{-r/l_h} - \frac{m_e}{\Delta m} e^{-r/l_e} \right), \quad (3)$$

with $\Delta m = m_h - m_e$. This potential was derived assuming $l_{e,h}$ that the polaron lengths are much smaller than the effective exciton radius, which entered as a variational parameter in the original calculations.²⁸ The bare band electron and hole masses must be used in the kinetic energy terms of the PB Hamiltonian.

In the present work, the exciton energies are obtained solving the radial Schrödinger equation for the relative coordinate wave function of the exciton $\Phi(r)$

$$\frac{d^2\Phi}{dr^2} + \frac{2}{r} \frac{d\Phi}{dr} + \left(\frac{2\mu}{\hbar^2} (E - V(r)) - \frac{l(l+1)}{r^2} \right) \Phi = 0, \quad (4)$$

where $V(r)$ is the electron-hole interaction potential (Coulomb, Haken, or PB), l is the azimuthal quantum number, of which we only consider $l = 0$ that are the optically active states. The Eq. (4) for $l = 0$ has been solved integrating the equation starting from $r = 0$ with the conditions $\Phi(0) > 0$, $\Phi'(0) = 0$ and imposing $\Phi(r_c) = 0$, where r_c is a cutoff radius sufficiently large to mimic the boundary conditions at infinity. The cutoff radii r_c are established solving the equation for the Coulomb potentials and comparing the numerical energies with the known exact solutions. We have used exciton atomic units a_0 and Ry_0 for the radius and energy, respectively. The functions are normalized according to

$$\int_0^{r_c} 4\pi |\Phi(r)|^2 r^2 dr = 1. \quad (5)$$

The optical oscillator strengths are defined as

$$f_n = \frac{2m_0}{\hbar\omega_{n,0}} |\langle \Psi_n | \vec{\xi} \cdot \hat{v} | 0 \rangle|^2, \quad (6)$$

TABLE I. Parameters defining the polarons in $\text{CH}_3\text{NH}_3\text{PbI}_3$.

Dielectric constants	
ϵ_∞	5.32 ^a
$\epsilon_\infty/\epsilon_0$	0.236 ^b
LO phonon energy	
E_{LO}	38.5 meV ^c
Coupling constants	
α_e	1.18
α_h	1.28
Bare carrier masses	
m_e/m_0 ^a	0.190
m_h/m_0 ^a	0.225
Polaron masses	
m_e^*/m_0	0.228
m_h^*/m_0	0.273
Polaron radii	
l_e	22.83 Å
l_h	21.00 Å
Polaron shift	
ΔE_p^e	-45.3 meV ^a
ΔE_p^h	-49.2 meV ^a

^a Ref. 15.^b Ref. 22.^c Ref. 29.

where m_0 is the free electron mass, $\hbar\omega_{n,0} = Eg^* + E_n$ is the transition energy, $|0\rangle$ and $|\Psi_n\rangle$ are the ground and excited states of the crystal, respectively, and $\hat{v} = i[\hat{H}, \hat{r}]/\hbar$ is the velocity operator.³² E_g^* is the renormalized gap (with the polaron shift), and E_n are the eigenvalues of Eq. (4). We shall approximate f_n by the expression for pure excitons, i.e., neglecting the phonon coupling, as

$$f_n = \frac{2m_0}{\hbar\omega_{n,0}} \sum_{cv} \sum_{\alpha=x,y,z} \frac{1}{3} |\langle u_{c0} | \hat{v}_\alpha | u_{v0} \rangle|^2 \frac{\Omega_{f.u.}}{a_0^3} |\Phi_n(0)|^2. \quad (7)$$

In the above expression, $\Omega_{f.u.}$ is the normalization volume of the center-of-mass part of the exciton envelope wave function, which we consider as the volume of one formula unit, i.e., one fourth of the unit cell volume 952.5 Å³. With this convention, the oscillator strength is equivalent to the values reported elsewhere.^{16,18} The factor 1/3 and the sum in α correspond to isotropic average of the crystal orientations. u_{v0} and u_{c0} are the Bloch functions of the valence band maximum and conduction band minimum, which in this case are both doubly degenerate. Using first principles calculations (see the Appendix) we have calculated the parameter

$$U_{cv} = \frac{m_0}{2} \sum_{cv} \sum_{\alpha=x,y,z} \frac{1}{3} |\langle u_{c0} | \hat{v}_\alpha | u_{v0} \rangle|^2 = 1.706 \text{ eV}. \quad (8)$$

Therefore, we obtain the simplified expression

$$f_n = \frac{4U_{cv}}{\hbar\omega_{n,0}} \frac{\Omega_{f.u.}}{a_0^3} |\Phi_n(0)|^2. \quad (9)$$

Let us stress that the exciton Bohr radius a_0^3 appears in Eq. (9) only if the normalization condition (5) is applied in relative units of a_0 .

Both the Haken and Pollmann-Büttner potentials behave like a Coulomb potential for very large distance ($r \gg l_e, l_h$) or very short distances ($r \ll l_e, l_h$), screened by the low and high frequencies dielectric constants, respectively. Figure 1 shows in logarithmic scale, the limiting Coulomb potentials screened by ϵ_0 and ϵ_∞ . These are represented by the straight lines, enclosing the Haken and Pollmann-Büttner potentials, that interpolate the limiting cases. Horizontal lines represent the eigenenergies of the exciton relative motion. The axes in the figure are in units of static (fully screened) exciton radius and $a_0 = \hbar^2\epsilon_0/\mu e^2$ and exciton energy $Ry_0 = \mu e^4/2\hbar^2\epsilon^2$. In these units, the static Coulomb potential is given by $-2/r$ and the exciton eigenenergies are $E_n^0 = -1/n^2$. The Coulomb potential and the hydrogenic energies defined by ϵ_∞ are $E_n^\infty = -\epsilon_r^2/n^2$, where $\epsilon_r = \epsilon_0/\epsilon_\infty$. For the parameters of $\text{CH}_3\text{NH}_3\text{PbI}_3$ ($\epsilon_r = 4.25$), one can appreciate in Figure 1 and Table II that the lowest exciton levels are $E_n^H = -11.26$ and $E_n^{PB} = -8.65$ for the Haken and PB potentials. These values represent a significant correction to either $E_1^0 = -1$ or $E_1^\infty = -18$. The excited exciton energies of Haken and PB potentials approach the values $-1/n^2$ for high n .

In order to compare the energies E_1^H and E_1^{PB} one must consider that Ry_0 is defined either by the polaron or the bare reduced mass in the first and second model, respectively. In absolute units, $E_1^H = -37$ meV and $E_1^{PB} = -24$ meV. It seems that the PB value is in better agreement with the experimental values near 19 meV.^{23,25}

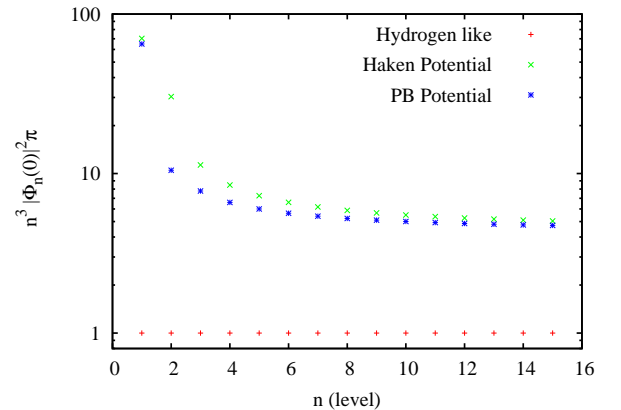


FIG. 2. Oscillator strengths of polaron excitons and hydrogenic exciton.

The values of $\Phi(0)$ in Table II and Figure 2 shows that the ground exciton is optically active. According to

TABLE II. Exciton binding energies and wave function at origin. The wave function is normalized with the radii in units of a_0 . In the same units, the hydrogenic functions fulfill $\Phi_n^0(0) = 1/\sqrt{\pi n^3}$. In normal units, $\Phi_n(0)$ must be divided by $a_0^{3/2}$.

n	Haken model		PB model	
	E_n^H/Ry_0	$\Phi_n^H(0)$	E_n^{PB}/Ry_0	$\Phi_n^{PB}(0)$
1	-11.2605	4.7255	-8.6473	4.5421
2	-0.8128	1.0832	-0.4622	0.6507
3	-0.2092	0.3636	-0.1661	0.3031
4	-0.0979	0.2047	-0.0839	0.1811
5	-0.0567	0.1358	-0.0505	0.1236
6	-0.0370	0.0985	-0.0337	0.0911
7	-0.0260	0.0756	-0.0240	0.0708
8	-0.0193	0.0604	-0.0180	0.0570
9	-0.0149	0.0497	-0.0140	0.0472
10	-0.0118	0.0418	-0.0112	0.0399
11	-0.0096	0.0358	-0.0092	0.0343
12	-0.0080	0.0311	-0.0076	0.0299
13	-0.0067	0.0274	-0.0065	0.0264
14	-0.0057	0.0243	-0.0055	0.0235
15	-0.0050	0.0218	-0.0048	0.0211

Eq. (9) the oscillator strength in the PB model is 0.013. The second exciton level is only 2.7 meV (Haken) or 1.2 meV (PB) below the edge of the continuum spectrum, and their oscillator strengths are one order of magnitude smaller than for the main line ($n = 1$), making these transitions practically undetectable in the optical spectra. Higher energies approach to the sequence $E_g - Ry_0/n^2$. For these higher levels, the oscillator strengths become proportional to the hydrogenic oscillator strengths. The proportionality constant is fitted to $\beta_H = 4.282$ (Haken) and $\beta_{PB} = 4.214$ (PB) in each case. The fitting function was $f(n) = \beta + \gamma/(n - n_0)$, and the fitted β are stable for any subset of data with $n > 7$. Let us note that

$$\beta \simeq \frac{\epsilon_0}{\epsilon_\infty}. \quad (10)$$

This result, together with the approximation of the energies by the sequence $E_g^* - Ry_0/n^2$, leads to a constant absorption spectrum near the band gap energy similar to the case of hydrogenic exciton,^{33,34}

$$\alpha(E_g^*) = \frac{2\pi e^2 \hbar P_{cv}^2}{E_g n_r c m_0^2} \frac{\beta}{a_0^3 Ry_0}, \quad (11)$$

where n_r is the refraction index and can be approximated by $\sqrt{\epsilon_\infty}$. Evaluation of the physical constants, and using Eqs. (10), (8), and (A5), the above expression can be cast as

$$\alpha(E_g^*) = (3.466 \text{ nm}^{-1}) \frac{U_{cv}}{n_r E_g} \left(\frac{\mu}{m_0} \right)^2 \frac{1}{\epsilon_\infty}, \quad (12)$$

Using the material parameters of $\text{CH}_3\text{NH}_3\text{PbI}_3$, $\alpha(E_g) \sim 3.1 \mu\text{m}^{-1}$.

The exciton spectrum obtained presents of a low energy non-hydrogenic state that is 37 or 24 meV (in Haken or PB models, respectively) below the onset of continuous free polaron spectrum. The rest of the discrete exciton spectrum resembles the hydrogenic series with static dielectric constant ϵ_0 . The first exciton state dominates the absorption edge with oscillator strength ~ 0.013 , while the oscillator strengths of higher states are one or two orders of magnitude smaller. Like the case of hydrogenic exciton, the coalescence of absorption lines from higher states generates a quasi-continuum spectrum with a finite value at the gap energy. The absorption coefficient at gap energy is enhanced with respect to the hydrogenic model by a factor $\epsilon_0/\epsilon_\infty$. Extrapolating this behavior to the room temperature tetragonal phase, this enhancement factor could be responsible of the high capacity of this material to collect the photon energy in the photovoltaic cells.

To interpret the absorption experiments and to determine de band gap, one needs to know whether the onset of the continuous absorption spectrum corresponds to the exciton continuum spectrum, or to the accumulation of discrete lines below the band gap. In other words, what is the energy range of constant absorption coefficient given by Eq. (12). Considering that the higher exciton levels are within 2 meV of the continuum, and that the exciton absorption spectrum is dominated by the fundamental state, one can conclude that the band gap coincides with the absorption threshold after filtering the first exciton peak. On the other hand, the polaronic effect downshifts the gap by 95 meV. Therefore, the measured gap 1.68 eV should be understood as an electronic gap of 1.78 eV decreased by the polaron shift.

Several kinds of estimations of the exciton binding energy in $\text{CH}_3\text{NH}_3\text{PbI}_3$ have been reported. The first method was employed by Hirasawa et al.,¹⁷ and repeated later with improved accuracy by Tanaka et al.¹⁸ They measured the exciton diamagnetic coefficient in magneto-absorption spectra, and related the measurements with the binding energy in the framework of the hydrogenic model with the high frequency dielectric constant. With this model, Tanaka et al determined a binding energy of 50 meV. The use of the high frequency dielectric constants was a choice of the model, and not determined by the experiments. Let us note that Tanaka et al, and Hirasawa et al used a value $\epsilon_\infty = 6.5$ that is higher than our value. If our value $\epsilon_\infty = 5.32$ were used, a binding energy of 65 meV would be obtained. Conversely, our binding energies using the larger dielectric constant would be smaller. These values of the exciton binding energy are strongly biased by the choice of the dielectric constants.

The second method has been applied by Sun et al²³ ($E_B = 19$ meV). They obtained the binding energy by fitting the photoluminescence intensity as a function of temperature with an Arrhenius equation, not using

any model of the exciton states. It is rewarding that our calculation of the binding energy is in good agreement with the values determined by Sun et al. Huang and Lambrecht³⁵ have argued, in a study of cesium tin halide perovskites, that the photoluminescence temperature dependence just give information on the free exciton linewidth or the binding energies of bound excitons, but not on free excitons. However, Even et al²⁴ fitted the absorption spectrum using the Wannier-Mott exciton model and obtained a similar value for the binding energy, and reported an effective dielectric constant $\epsilon_{eff} = 11$. This value of the dielectric constants, together with the assumed reduced mass $0.16m_0$ ²⁴ means a binding energy of 19 meV. Another method independent of the dielectric function has been used by Miyata et al,²⁵ who performed magneto-absorption experiments with very high magnetic fields, determining a value of 16 ± 2 eV. It is interesting that Miyata et al were able to detect the $2s$ exciton state for high magnetic field and extrapolated a $1s - 2s$ difference of 15 meV at low magnetic field. Henceforth, assuming the hydrogenic model, they estimated the binding energy in 20 meV. However, extrapolating the Landau levels of the free exciton spectrum they obtained the precise value of 16 meV. This observation agrees with our result that the $2s$ state is within 2 meV of the free exciton edge.

The evaluation of the oscillator strength provides another argument against the model of hydrogenic Wannier excitons screened by ϵ_0 . Ishihara¹⁶ reported an experimental values of 0.02, which is close to our value 0.013. If the ground exciton were well described by hydrogenic model with ϵ_0 , then $\Phi_1(0) = 1/\sqrt{\pi}$ (compare with Table II and Fig. 2), and the oscillator strength would be ~ 64 times smaller. Therefore, at least for low temperature, the fundamental exciton state does not correspond to screening by ϵ_0 .

We wish to stress that we have not fitted any parameter in this work, which would bring the exciton binding energies in closer agreement with the recent experimental results. The parameters with larger uncertainty are the dielectric constants and the LO phonon energy. The only available experimental value of $\epsilon_\infty = 6.5$ ¹⁷ is larger than the ab initio value used here and that value would reduce the calculated binding energy. The measurement of ϵ_∞ is rather old, with few published details, and a new determination for present-day thin films would be welcomed. The LO phonon energy E_{LO} has been chosen from the more prominent peak in the calculated Raman spectrum of $\text{CH}_3\text{NH}_3\text{PbI}_3$,²⁹ which is close to LO phonon energies in II-VI and III-V semiconductors. As mentioned above, the model Hamiltonians were developed assuming a unique LO phonon energy. The Raman spectrum of $\text{CH}_3\text{NH}_3\text{PbI}_3$ shows bands at lower wave numbers. Using and average energy of the Raman active peaks, which do not have necessarily LO character, may lead to lower exciton binding energy. An extension of the PB Hamiltonian to include several LO phonon branches would be a better founded approach.

In summary, we have calculated the exciton binding energies and oscillator strengths using two model Hamiltonians of the exciton-phonon coupled system. The Pollmann-Büttner model Hamiltonian gives a binding energy in good agreement with recent experimental determinations. The calculated oscillator strength of the main exciton line agrees with the value estimated from experiments, while the strengths of higher transitions are much smaller.

ACKNOWLEDGMENTS

We acknowledge computer time from the Jülich Supercomputing Centre (JSC) under the MOHP-SOPHIA project, and support from FONDECYT Grant. No. 1150538 and the European Project NANOCIS of the FP7-PEOPLE-2010-IRSES. We acknowledge J. C. Conesa, P. Palacios and C. Trallero-Giner for interesting discussions that motivated this work.

Appendix A: Interband matrix element

With the VASP code³⁶ the tensor dielectric function is computed in the longitudinal approximation³⁷

$$\varepsilon_{\alpha\beta}^{(2)}(\omega) = \frac{4\pi^2 e^2}{\Omega} \lim_{q \rightarrow 0} \frac{1}{q^2} \sum_{c,v,\mathbf{k}} g_S w_{\mathbf{k}} \delta(\epsilon_{c\mathbf{k}+\mathbf{q}} - \epsilon_{v\mathbf{k}} - \hbar\omega) \times \langle u_{c\mathbf{k}+\mathbf{e}_\alpha q} | u_{v\mathbf{k}} \rangle \langle u_{c\mathbf{k}+\mathbf{e}_\beta q} | u_{v\mathbf{k}} \rangle^*, \quad (\text{A1})$$

where $w_{\mathbf{k}}$ are the k-point weights, defined such that they sum to 1, $\epsilon_{c\mathbf{k}+\mathbf{q}}$ are band energies, Ω is the unit cell volume, m_0 is the vacuum electron mass, \mathbf{e}_α are polarization vectors. The factor g_S is the spin degeneracy, which is 2 in Ref. 37, and the bands v, c in the sum are restricted to have the same spin. In the calculation with spin-orbit coupling, we consider $g_S = 1$ and the sum is over all pairs of valence and conduction bands. The Eq. A1 is equivalent to the transverse approximation,³²

$$\varepsilon_{\alpha\beta}^{(2)}(\omega) = \frac{4\pi^2 e^2}{\Omega \omega^2} \sum_{c,v,\mathbf{k}} g_S w_{\mathbf{k}} \delta(\epsilon_{c\mathbf{k}} - \epsilon_{v\mathbf{k}} - \hbar\omega) \times \langle u_{c\mathbf{k}} | \hat{v}_\alpha + \frac{\hbar k_\alpha}{m_0} | u_{v\mathbf{k}} \rangle \langle u_{c\mathbf{k}} | \hat{v}_\beta + \frac{\hbar k_\beta}{m_0} | u_{v\mathbf{k}} \rangle^*. \quad (\text{A2})$$

For a local Hamiltonians with spin-orbit coupling, $m_0 \hat{v} = -i\hbar \nabla + (\hbar/4m_0 c^2) \vec{\sigma} \times \nabla V$. The PAW potentials and the hybrid functionals introduce non-locality in the Hamiltonian, and the velocity operator contains additional terms.³² For the purpose of the optical properties of the exciton, we only need the values of $\langle u_{c\mathbf{k}} | \hat{v}_\beta | u_{v\mathbf{k}} \rangle$ between the VBM and the CBM, which occurs at the Γ point ($k_\beta = 0$). These values $\langle u_{c\mathbf{k}} | \hat{v}_\beta | u_{v\mathbf{k}} \rangle$ can be fitted from the dielectric function, which is calculated using (A1). Hence, if the contribution of the Γ point can be

separated from the other k-point contributions, we have that

$$\varepsilon_{\alpha\beta;\Gamma}^{(2)}(\omega) = \frac{4\pi^2 e^2}{\Omega\omega^2} g_S w_0 \sum_{cv} \delta(\epsilon_{c\mathbf{0}} - \epsilon_{v\mathbf{0}} - \hbar\omega) \times \langle u_{c\mathbf{0}} | \hat{v}_\alpha | u_{v\mathbf{0}} \rangle \langle u_{c\mathbf{0}} | \hat{v}_\beta | u_{v\mathbf{0}} \rangle^*. \quad (\text{A3})$$

In the above expression, the sum \sum' is restricted to the top valence bands and bottom valence bands.

To fit with the exciton, we consider the averaged dielectric function $\varepsilon = (1/3)\text{Tr}\varepsilon_{\alpha\alpha}$

$$\varepsilon_\Gamma^{(2)}(\omega) = \frac{4\pi^2 e^2}{\Omega\omega^2 m_0^2} g_S w_0 P_{cv}^2 \delta(\epsilon_{c\mathbf{0}} - \epsilon_{v\mathbf{0}} - \hbar\omega), \quad (\text{A4})$$

with

$$P_{cv}^2 = \frac{1}{3} \sum_\alpha \sum_{cv} |\langle u_{c\mathbf{0}} | m_0 \hat{v}_\alpha | u_{v\mathbf{0}} \rangle|^2. \quad (\text{A5})$$

The parameter P_{cv} has dimension of momentum, and $P_{cv}^2/2m_0$ is the parameter U_{cv} defined in Eq. (8).

In practical calculations, $\delta(\epsilon_{c\mathbf{0}} - \epsilon_{v\mathbf{0}} - \hbar\omega)$ is replaced by a smearing function. If gaussian smearing is used for the self-consistent calculation, the computed spectrum must be fitted with a Gaussian function weighted by $4\pi^2 e^2 g_S w_0 P_{cv}^2 / \Omega\omega^2 m_0^2$. The ab initio calculation was performed sampling the Brillouin zone with a $2 \times 2 \times 2$ k-point grid centered at the Γ point, which is sufficient to obtain total energies and charge densities, but it is coarse for calculation of optical properties and it allows to isolate the contributions of the Γ -point transitions. With this k-point mesh, the weight $w_0 = 1/8$. The details of the calculation are given in Ref. 15.

-
- ¹ A. Kojima, K. Teshima, Y. Shirai, and T. Miyasaka, J. Am. Chem. Soc. **131**, 6050 (2009).
 - ² (2015), NREL chart on record cell efficiencies, URL http://www.nrel.gov/ncpv/images/efficiency_chart.jpg.
 - ³ M. Jacoby, Chemical & Engineering News **92**, 21 (2014).
 - ⁴ L. Etgar, P. Gao, Z. Xue, Q. Peng, A. K. Chandiran, B. Liu, M. K. Nazeeruddin, and M. Grätzel, J. Am. Chem. Soc. **134**, 17396 (2012).
 - ⁵ N.-G. Park, J. Phys. Chem. Lett. **4**, 2423 (2013).
 - ⁶ O. Knop, R. E. Wasylshen, M. A. White, T. S. Cameron, and M. J. M. van Oort, Can. J. Chem. **68**, 412 (1990).
 - ⁷ T. Baikie, Y. Fang, J. M. Kadro, M. Schreyer, F. Wei, S. G. Mhaisalkar, M. Graetzel, and T. J. White, J. Mater. Chem. A **1**, 5628 (2013).
 - ⁸ C. C. Stoumpos, C. D. Malliakas, and M. G. Kanatzidis, Inorganic Chemistry **52**, 9019 (2013).
 - ⁹ Y. Kawamura, H. Mashiyama, and K. Hasebe, J. Phys. Soc. Jpn. **71**, 1694 (2002).
 - ¹⁰ R. E. Wasylshen, O. Knopp, and J. B. Macdonald, Solid State Commun. **56**, 581 (1985).
 - ¹¹ Q. Lin, A. Armin, R. C. R. Nagiri, P. L. Burn, and P. Meredith, Nature Phot. **9**, 106 (2015).
 - ¹² J. M. Frost, K. T. Butler, and A. Walsh, APL Materials **2**, 081506 (2014).
 - ¹³ P. Umari, E. Mosconi, and F. De Angelis, Sci. Rep. **4**, 4467 (2014).
 - ¹⁴ F. Brivio, K. T. Butler, A. Walsh, and M. van Schilfgaarde, Phys. Rev. B **89**, 155204 (2014).
 - ¹⁵ E. Menéndez-Proupin, P. Palacios, P. Wahnón, and J. C. Conesa, Phys. Rev. B **90**, 045207 (2014).
 - ¹⁶ T. Ishihara, J. Lumin. **60&61**, 269 (1994).
 - ¹⁷ M. Hirasawa, T. Ishihara, T. Goto, K. Uchida, and N. Miura, Physica B **201**, 427 (1994).
 - ¹⁸ K. Tanaka, T. Takahashi, T. Ban, T. Kondo, K. Uchida, and N. Miura, Solid State Commun. **127**, 619 (2003).
 - ¹⁹ V. D'Innocenzo, G. Grancini, M. J. P. Alcocer, A. R. S. Kandada, S. D. Stranks, M. M. Lee, G. Lanzani, H. J. Snaith, and A. Petrozza, Nat. Commun. **5**, 3586 (2014).
 - ²⁰ G. Wannier, Phys. Rev. **52**, 191 (1937).
 - ²¹ R. Knox, *Theory of excitons*, Solid State Physics: Supplement 5 (Academic Press, 1963).
 - ²² F. Brivio, A. B. Walker, and A. Walsh, APL Materials **1**, 042111 (pages 5) (2013).
 - ²³ S. Sun, T. Salim, N. Mathews, M. Duchamp, C. Boothroyd, G. Xing, T. C. Sumbce, and Y. M. Lam, Energy Environ. Sci. **7**, 399 (2014).
 - ²⁴ J. Even, L. Pedesseau, and C. Katan, J. Phys. Chem. C **118**, 11566 (2014).
 - ²⁵ A. Miyata, A. Mitouglu, P. Plochocka, O. Portugall, J. T.-W. Wang, S. D. Stranks, H. J. Snaith, and R. J. Nicholas, Nature Phys. (2015), doi:10.1038/nphys3357, arXiv:1504.07025.
 - ²⁶ H. Haken, Z. Phys. **146**, 527 (1956), ISSN 0044-3328.
 - ²⁷ H. Haken, Fortschr. Phys. **6**, 271 (1958).
 - ²⁸ J. Pollmann and H. Büttner, Phys. Rev. B **16**, 4480 (1977).
 - ²⁹ C. Quarti, G. Grancini, E. Mosconi, P. Bruno, J. M. Ball, M. M. Lee, H. J. Snaith, A. Petrozza, and F. De Angelis, J. Phys. Chem. Lett. **5**, 279 (2014).
 - ³⁰ J. T. Devreese and A. S. Alexandrov, Rep. Prog. Phys. **72**, 066501 (pages 55) (2009).
 - ³¹ H. Haken, J. Phys. Radium **17**, 826 (1956).
 - ³² R. Del Sole and R. Girlanda, Phys. Rev. B **48**, 11789 (1993).
 - ³³ G. Grosso and G. Pastori-Parravicini, *Solid State Physics* (Academic Press, San Diego, 2000), 1st ed.
 - ³⁴ R. J. Elliot, Phys. Rev. **108**, 1384 (1957).
 - ³⁵ L.-Y. Huang and W. R. L. Lambrecht, Phys. Rev. B **88**, 165203 (2013).
 - ³⁶ G. Kresse and J. Furthmüller, Phys. Rev. B **54**, 11169 (1996).
 - ³⁷ M. Gajdoš, K. Hummer, G. Kresse, J. Furthmüller, and F. Bechstedt, Phys. Rev. B **73**, 045112 (2006).